PHYSICAL AND ANALITICAL CHEMISTRY

Mudar A. Abdulsattar[1] [iD][*], Sawsan M. Almaroof[2]

[1]*Ministry of Science and Technology, Baghdad, Iraq;*
[2]*Engineering Construction Office, Ministry of Construction, Housing, Municipalities and Public Works, Baghdad, Iraq*
*(*Corresponding author′s e-mail: mudarahmed3@yahoo.com)*

H$_2$S Properties and Temperature Effects
on the Response of Pristine and Al-Doped ZnO Gas Sensor

H$_2$S is a poisonous gas that needs to be censored to protect humans from its exposure. H$_2$S gas sensitivity and interaction with pristine and Al-doped ZnO clusters were studied using the transition state theory method. The reaction of ZnO with H$_2$S gas is usually weak and can be enhanced by doping. Elements or their oxides, such as platinum group elements, are traditionally used as doping substances. However, the use of other cheaper elements or oxides such as Al or Mn also increases the reaction rate. The mechanism of increasing the reaction rate and sensitivity by Al doping is the subject of present work. The calculation results show that Al-doped ZnO increases the sensitivity towards H$_2$S by growing the resistance of Al-doped ZnO due to lattice distortion. The Gibbs activation energy remains almost the same as calculated by the present model. In conclusion, it should be noted that good agreement between theory and experiment was achieved in terms of temperature-dependent reaction rate, gas response, recovery and response time for different doping ratios. For the first time, the autoignition reaction and temperature of H$_2$S were considered in sensors. Further improvement in transition state theory is needed to include further gas sensor features.

Keywords: Al doping, ZnO cluster, pristine, H$_2$S gas sensor, DFT, transition state, autoignition temperature, activation energy

Introduction

Zinc oxide is one of the most studied materials in the scientific literature due to its unique properties and wide application [1], such as paints, cosmetics, rubber, composites, etc. One of its applications is as a gas sensor [2]. ZnO is used to monitor gases such as ethanol [3], CO$_2$ [4], NO$_2$ [5], H$_2$S [6] etc. The response of pure ZnO or other pure compounds can be enhanced by doping. Platinum group elements such as ruthenium, rhodium, and palladium are usually most effective in addition to other transition elements [7, 8]. The response enhancement is generally explained by the reduction of activation energy needed for the reaction between the gas and sensitive material to proceed [9, 10]. However, cheaper doping with non-transition elements enhances the sensor's response to the targeted gas [6, 11]. Optimized ZnO small molecules, which resemble the wurtzite lattice structure, can be used to study the behavior of ZnO properties and reactions [12, 13]. The most appropriate molecule in terms of size and computation time is Zn$_{13}$O$_{13}$, called ZnO wurtzoid2c [14].

Hydrogen sulfide is a poisonous gas that reacts with the human body or materials, so it must be monitored [15]. H$_2$S can be explosive when its concentration exceeds certain limits in air [16]. The electronic structure and shape of the H$_2$S molecule are similar to the structure and shape of the water molecule, in which oxygen is replaced by sulfur. H$_2$S can be ignited by an external ignition source if its temperature exceeds its flash point temperature at –82 °C [17]. However, H$_2$S can explode at temperatures above its au-

toignition temperature of 232 °C without an external ignition source [17]. H$_2$S can be removed from fuel using ZnO [18, 19], so it is natural to expect that ZnO will be used as a H$_2$S gas detector [20, 21].

Despite the substantial experimental literature on gas sensors, including thousands of scientific papers [22, 23], theoretical studies related to gas sensors are limited to a few gases and gas-sensitive materials. A common theoretical approach involves density functional theory (DFT) for gas sensing analysis [22, 23]. Theoretical modeling of the reaction is carried out using either the Arrhenius equation or the more modern transition state theory [10].

This study uses transition state theory and DFT to investigate pure or Al-doped ZnO as an H$_2$S gas sensor. The H$_2$S reaction rate and response temperature dependence are compared with existing experiment. Response and recovery time trends are also compared to available experiment.

Computational Details and Theoretical Background

Gaussian 09 software was used to perform present calculations [24]. The calculation used B3LYD theory level of DFT and 6-311G** basis set. Gas reaction with solids usually contains long-range forces that enforce dispersion corrections. Dispersion corrections at the GD3BJ level are used successfully in previous and present calculations [10].

The removal of H$_2$S from fuel or biological materials using ZnO is a well-known process [18, 19] which can be represented by the following reaction:

$$ZnO + H_2S \rightarrow ZnS + H_2O. \tag{1}$$

In the above reaction, sulfur replaces oxygen in the ZnO lattice. Figure 1a shows the adsorption of the H$_2$S molecule on the Zn$_{13}$O$_{13}$ molecule (denoted [Zn$_{13}$O$_{13}$—H$_2$S]^a). It should be noted that the H$_2$S molecule loses one of its hydrogen atoms simultaneously with adsorption.
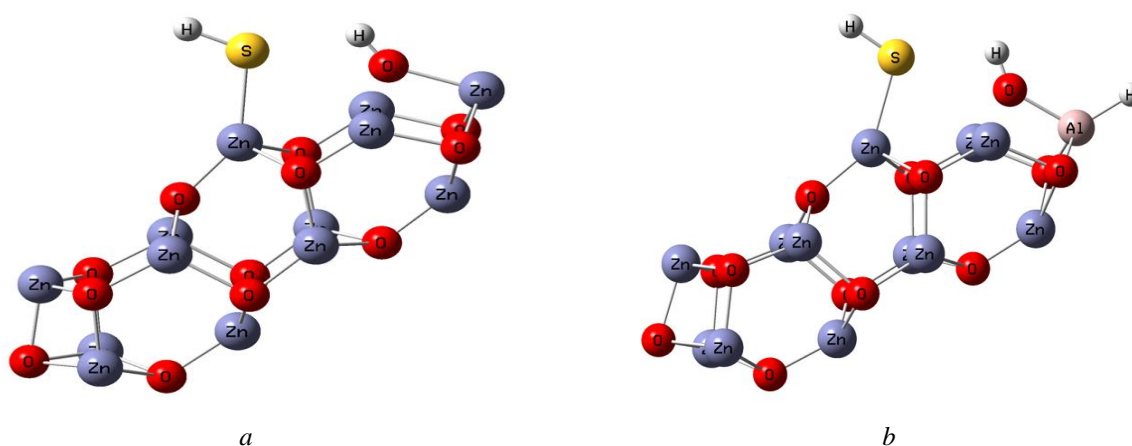
Figure 1. a — optimized geometry of Zn$_{13}$O$_{13}$ cluster with adsorbed H$_2$S molecule ([Zn$_{13}$O$_{13}$—H$_2$S]^a); b — optimized geometry HAlZn$_{12}$O$_{13}$ cluster with adsorbed H$_2$S gas ([HAlZn$_{12}$O$_{13}$—H$_2$S]^a)

Figure 1b shows the effect of H$_2$S adsorption when one Zn atom is replaced by aluminum in Zn$_{13}$O$_{13}$ (denoted HAlZn$_{12}$O$_{13}$—H$_2$S]^a). A hydrogen atom was added to the Al-doped molecule to compensate the difference in oxidation state of Al(+3) and Zn(+2).

The transition state is the state of the highest potential energy along the reaction coordinates. A double dagger is added to this state to differentiate it from other states (denoted [Zn$_{13}$O$_{13}$—H$_2$S]‡). The slight movement of atoms in the transition state decreases its molecular Gibbs free energy ($\Delta G^‡$) by 0.0617 eV for the pure and 0.0581 eV for the Al-doped ZnO molecule in normal temperature and pressure, as shown in Figure 2.

In transition state theory, the reaction rate of H$_2$S gas with ZnO can be determined by the formula [25–27]:

$$\frac{d[ZnO]}{dt} = -[ZnO]\,[H_2S]_e\,k(T), \tag{2}$$

$$k(T) = AT^m \exp\left(\frac{-\Delta G^‡}{k_B T}\right). \tag{3}$$

In the above equations, [ZnO] and $[H_2S]_e$ are the ZnO and H_2S gas concentrations, respectively. The subscript (e) in $[H_2S]_e$ concentration indicates the effective available concentration due to H_2S burning in high temperatures as it approaches the autoignition temperature. $k(T)$ is the temperature-dependent term in the rate equation. k_B is the Boltzmann constant. A in Eq. (3) is a scaling constant corresponding to the sensitive material's area in the experiment. The value of the temperature exponent (m) in (T^m) can be fit to experimental results and depends on the type of interacting materials and diffusion of reaction gases. The Gibbs free energy of transition $(\Delta G^\ddagger)$ is related to the enthalpy of transition $(\Delta H^\ddagger)$ and entropy of transition $(\Delta S^\ddagger)$ by the equation:

$$\Delta G^\ddagger = \Delta H^\ddagger - T\Delta S^\ddagger . \tag{4}$$

The Gibbs free energy of the transition is usually impossible to obtain with the required ratio of ingredients due to computational size problems. This problem can be solved using the modified Evans–Polanyi principle [10]:

$$\Delta G^\ddagger = \Delta G_0^\ddagger + \beta\Delta G_1^\ddagger . \tag{5}$$

In Eq. (5), $\Delta G_0^\ddagger$ and $\Delta G_1^\ddagger$ there are two known values of the Gibbs free energy of activation for specific concentrations of the dopants. These points can be used to obtain $\Delta G^\ddagger$ through the interpolation parameter β. The above equation is a modification of the Evans–Polanyi principle with the inclusion of entropy in the formalism [10, 28].

A logistic function can be used to account for the decrease in H_2S gas content as it approaches the autoignition temperature of 232 °C:

$$f(T) = \frac{1}{1 + e^{k_s(T - T_0)}} . \tag{6}$$

In Eq. (6), k_s is the steepness of the decrease in H_2S concentration, while T_0 is the temperature at which H_2S reaches half of its concentration.

The experimental sensitivity of a gas sensor is obtained by dividing the resistance of the sensor in the air (R_a) by the resistance when the detected gas (H_2S) is added (R_g). This ratio (R_a/R_g) is proportional to the calculated reaction rate:

$$\text{Response(theoretical)} = 1 + C\left|\frac{d[\text{ZnO}]}{dt}\right| . \tag{7}$$

C in the above equation is the proportionality constant, and a value of one (1) is added to account for the response value in the absence of the detected gas.

The most important parts of any theory are the results that can be compared to experiments. In gas sensors, 90 % of the response and recovery time corresponds to the moment when the resistivity changes to 90 % of its original resistance.

By integrating Eq. (2), the 90 % of response time can be determined by the formula:

$$t_{res(90\%)} = \frac{\ln(10)}{[\text{H}_2\text{S}]_e \, AT^m \, \exp^{\left(\frac{-G^\ddagger}{k_B T}\right)}} . \tag{8}$$

On the other hand, the 90 % of recovery time is the time that corresponds to the return of the resistivity to 90 % of its original value. This time corresponds to the oxygen retrieval of the oxygen-reduced ZnO, as in the reaction:

$$\text{Zn}_{13}\text{O}_{12} + \tfrac{1}{2}\text{O}_2 \rightarrow \text{Zn}_{13}\text{O}_{13} . \tag{9}$$

In this case, the recovery time corresponding to the above reaction can be estimated using the equation:

$$t_{rec(90\%)} = \frac{\ln(10)}{[\text{O}_2]_e \, AT^m \, \exp^{\left(\frac{-G^\ddagger}{k_B T}\right)}} . \tag{10}$$
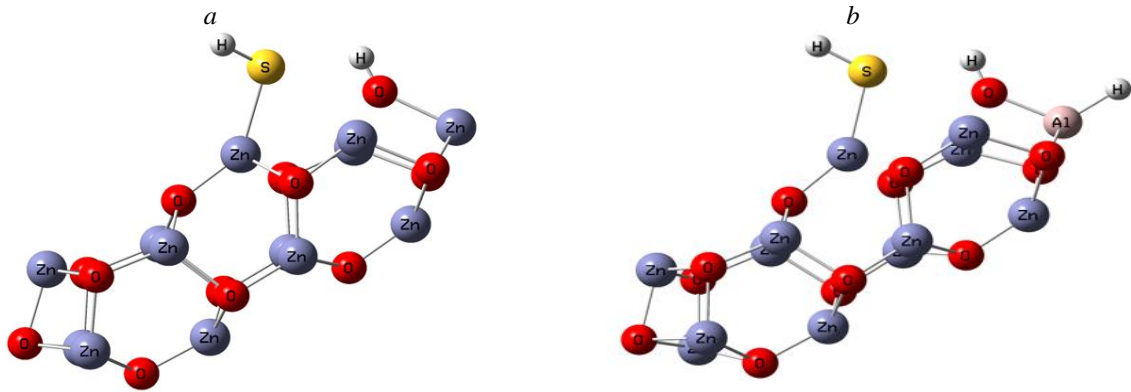
Figure 2. *a* — optimized geometry of transition state of adsorbed H$_2$S on Zn$_{13}$O$_{13}$ ([Zn$_{13}$O$_{13}$—H$_2$S]‡);
b — optimized geometry of transition state of HAlZn$_{12}$O$_{13}$ with H$_2$S gas ([HAlZn$_{12}$O$_{13}$—H$_2$S]‡)

Results and Discussion

Figure 3 shows the variation of Gibbs energy of transition as a function of temperature for pure ZnO doped with 2 % and 4 % Al (molar) upon absorption of H$_2$S gas.
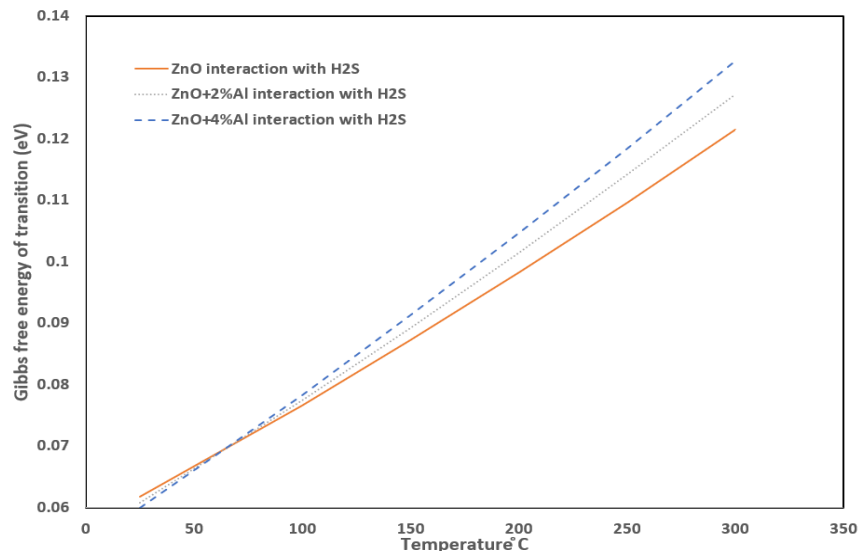
Figure 3. Gibbs free energy of transition for pure, 2 %, and 4 % Al doped ZnO
as a function of temperatures upon interaction with H$_2$S gas

As can be seen in Figure 3, the Gibbs energies are very close and intersect at low temperatures from 50 to 100 °C. The reason for the intersection is the increase in activation entropy of the doped ZnO [29]. This shows that the reaction rate is nearly equal in the pure and Al-doped ZnO. The increase in response in the Al-doped ZnO is mainly due to an increase in resistance due to doping. The imperfections in the lattice structure interact with electrons and increase resistivity. This increase has been proven for other binary systems as well [30].

Figure 4 shows the response of pure ZnO to H$_2$S.
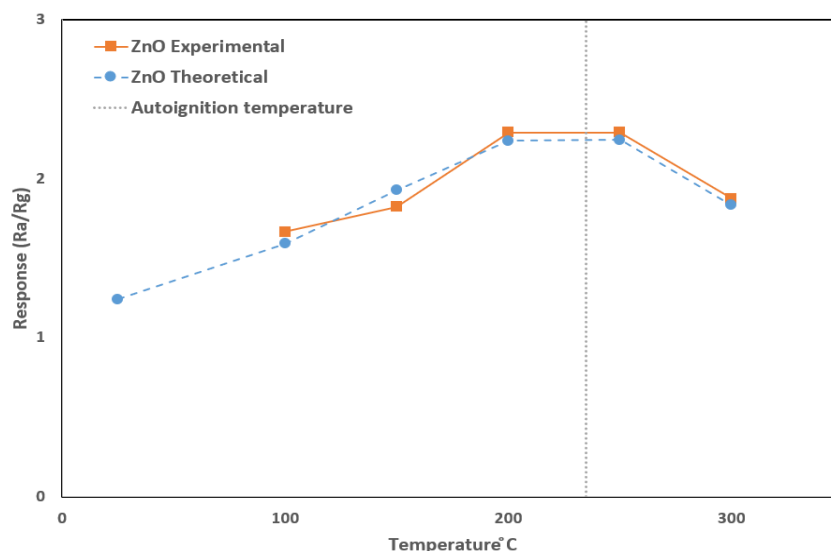
Figure 4. The experimental [6] and theoretically calculated responses of the pure ZnO sensor to 600 ppm H_2S gas at different temperatures. The autoignition temperature of H_2S gas [17] is indicated by the dotted line

As can be seen in Figure 4, pure ZnO responds poorly to H_2S gas due to difficulty in oxygen pick-up from its tight structure by H_2S gas. The theoretical temperature-dependent exponent part (T^m) in Eq. (3) is T^4. The temperature dependence is higher than the usual exponent (0 to 1) in different reaction theories. This temperature dependence is the hydrogen (in H_2S) fast diffusion into the ZnO structure. The autoignition temperature of H_2S gas is indicated in Figure 4, which shows the usual trend of optimum response temperature just before the autoignition temperature [11].

Figure 5 shows the response of 2 % Al (molar) doped ZnO.
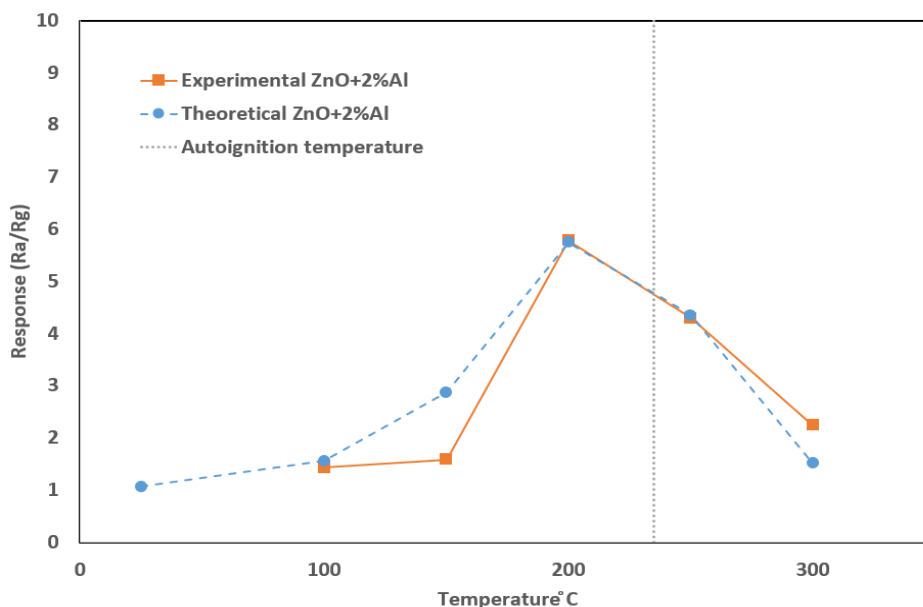
Figure 5. The experimental [6] and calculated theoretical responses of the 2 % Al (molar) doped ZnO sensor to 600 ppm H_2S gas at a range of temperatures. The autoignition temperature of H_2S gas [17] is indicated by the dotted line

As can be seen in Figure 5, the response of the 2 % Al doped ZnO is more than twice that of pure ZnO. The increase in response is because doping with 2 % Al destroys the periodic lattice structure of pure ZnO. The imperfections in the lattice structure interact with electrons and increase resistivity. The theoretical temperature exponent dependence (T^m) is also high with $m = 10$.

Figure 6 shows the response of 4 % Al (molar) doped ZnO.
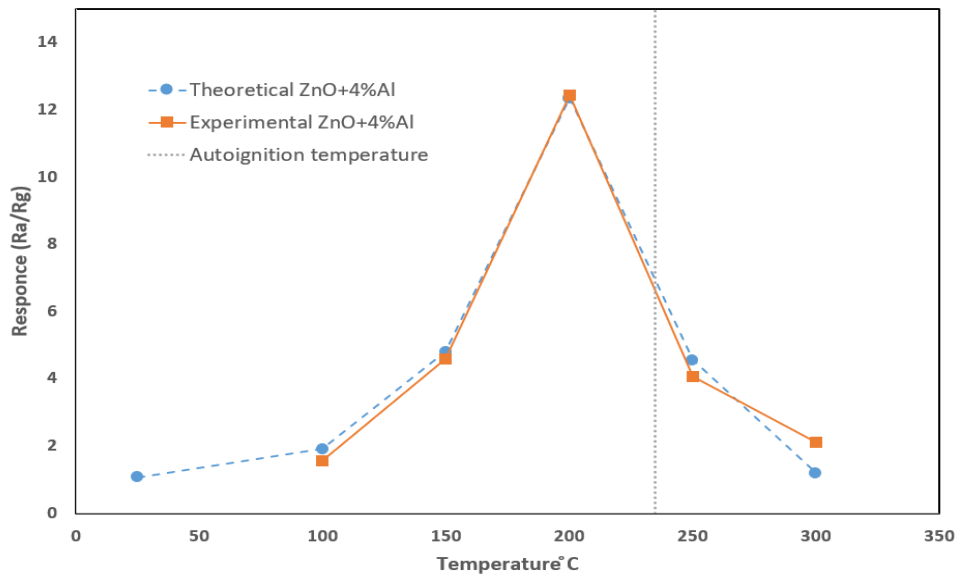
Figure 6. The experimental [6] and calculated theoretical responses of the 4 % Al (molar) doped ZnO sensor to 600 ppm H$_2$S gas at a range of temperatures. The autoignition temperature of H$_2$S gas [17] is indicated by the dotted line

As can be seen in Figure 6, the response of the 4 % Al doped ZnO is higher than pure and 2 % Al-doped ZnO. The 4 % Al-doped ZnO is near the highest possible response in Al-doped ZnO. As in the case of 2 % Al, the imperfections in the lattice structure interact with electrons and increase resistivity. The theoretical temperature exponent dependence (T^m) is also high with $m = 12$.

The three theoretical parts of Figures (4–6) show good agreement with experiments except for one point in Figure 5, that violets even the trend of the original experimental results [6].

The experimental response time data for the present system is scarce [6]. However, Figure 7 compares theoretical results and the experimental data available in reference [6] for the 4 % Al-doped ZnO. As shown in Figure 7, the 90 % response time is high except for a small range of temperatures. Theoretical results were obtained using Eq. (8).
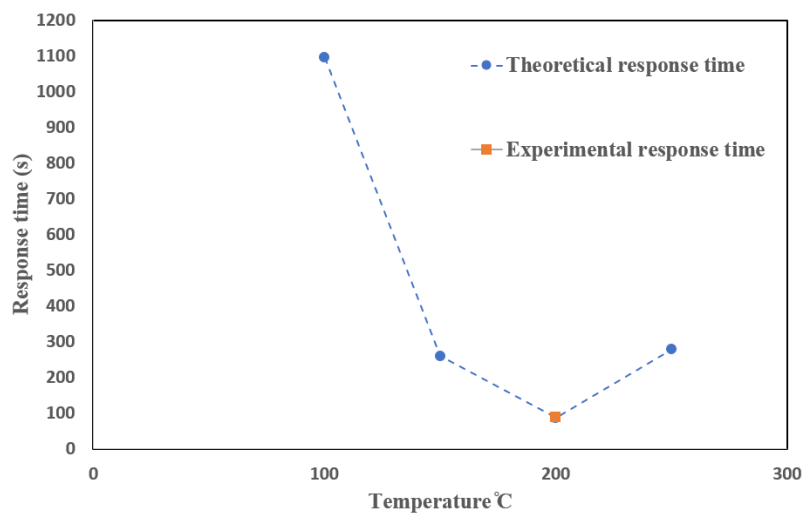
Figure 7. Response time of 4 % Al-doped ZnO at a range of temperatures for 600 ppm H$_2$S. Experimental data are taken from the reference [6]

At the recovery stage in the gas sensor in which atmospheric air (with no detected gas) passes over the sensitive material, the sulfurized surface of pure or Al-doped ZnO is desulfurized and re-oxidized as in the equations:

$$ZnS + O_2 \rightarrow Zn + SO_2 \tag{11}$$

$$Zn + \tfrac{1}{2}O_2 \rightarrow ZnO. \tag{12}$$
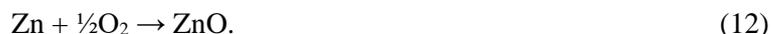
The desulfurization occurs in the response and recovery phase as well; however, at the end of the response phase, an oxygen-deficient ZnO surface occurs that will be oxidized in the recovery phase. Figure 8 shows the Gibbs free energy of the transition of oxygen-deficient pure and 4 % Al-doped ZnO as they interact with oxygen in the recovery phase.
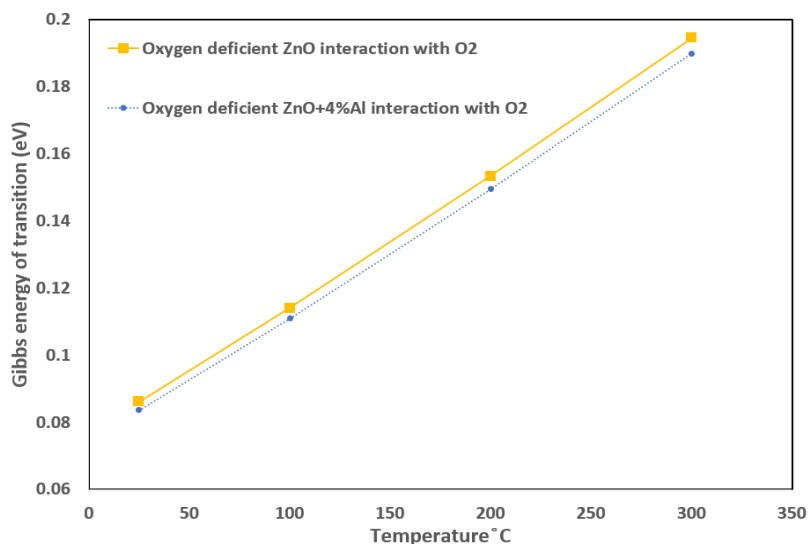
Figure 8. Gibbs free energy of the transition for pure oxygen-deficient and 4 % Al doped ZnO
as a function of temperatures as they interact with O_2

Figure 9 shows the recovery time of 4 % Al-doped ZnO to 600 ppm H_2S gas. The theoretical 90 % recovery time increases with temperature due to the increase in Gibbs free energy of transition as in Figure 8. The temperature exponent (T^m) in Eq. (10) is ($m = 0$). The negligible temperature exponent is due to the lack of oxygen diffusion into the ZnO structure.
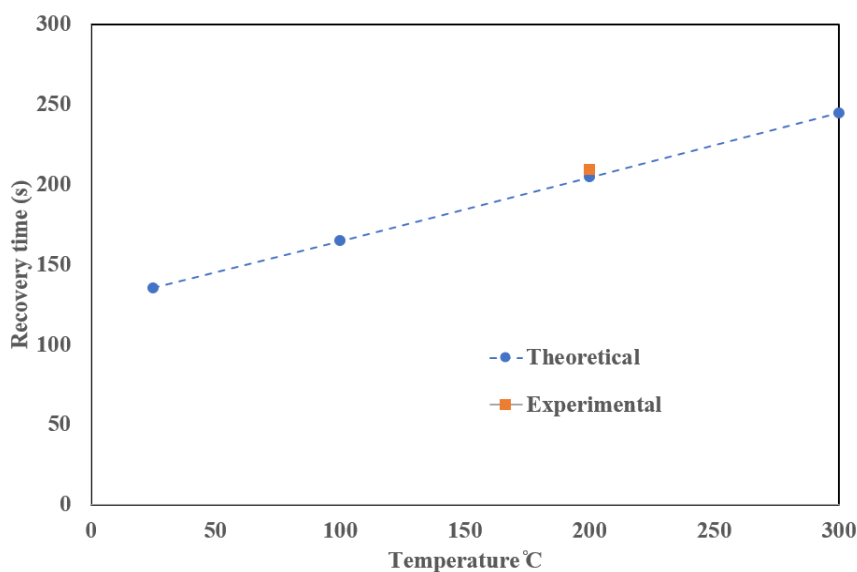
Figure 9. Recovery time of 4 % Al-doped ZnO as a function of temperature for 600 ppm H_2S.
Experimental data are taken from reference [6]

Table summarizes the Gibbs energy of transition and the five parameters used in each reaction corresponding to the several doping percentages and O_2 retrieval. The Gibbs free energy of transition is taken at 25℃ temperature and normal pressure. Gibbs energy of transitions for other temperatures is given in Figures 3 and 8.

T a b l e

Parameters used to simulate H₂S gas sensing and O₂ recovery reaction model of pure and Al-doped ZnO

No.	Reaction	$\Delta G^{\ddagger}$ (eV)*	A	m	k_s (K^{-1})	T_0 (°C)	C (s)
1	[ZnO—H₂S]^a ↓ [ZnO—H₂S]‡	0.0617	1.4 10^{-8} s^{-1}·K^{-4}	4	0.025	260	40
2	[2 % Al/ZnO—H₂S]^a ↓ [2 % Al/ZnO—H₂S]‡	0.0608	4.2 10^{-23} s^{-1}·K^{-10}	10	0.06	230	47
3	[4 % Al/ZnO—H₂S]^a ↓ [4 % Al/ZnO—H₂S]‡	0.0599	4.4 10^{-29} s^{-1}·K^{-12}	12	0.08	220	53
4	[4 % Al/Zn<u>O</u>—O₂]^a ↓ [4 % Al/Zn<u>O</u>—-O₂]‡	0.0836	2.1 s^{-1}	0	–	–	–
Note: $\Delta G^{\ddagger}$ values are at 25 °C temperature and normal pressure. An underscore is added to the oxygen in the fourth reaction to indicate an oxygen-deficient cluster of ZnO.							

It can be seen in Table that as the doping percentage increases, the Gibbs free energy of transition decreases. However, this is reversed as the temperature increases (as shown in Fig. 8) because of entropy, as explained previously. The parameter (A) has different units due to different temperature dependence and concentrations of each doping percentage. This is reflected by the exponent (m) that increases as the doping percentage increases. The parameter (A) for the fourth reaction differs from the first three reactions due to the difference in oxygen concentration (20 % of air) compared to ppm values of H₂S. The reason for the temperature exponent (m) increase in the reaction of H₂S gas with Al-doped ZnO is the distortion of the ZnO lattice due to doping. The distortion of the ZnO periodic lattice allows the H₂S gas to enter deeper (diffuse) and react with deep Al/ZnO layers, which makes the reaction more vigorous with the increase in temperature. In addition, since the Al oxidation state (3) is higher than Zn (2), several vacancies are created. Some vacancies are filled with atmospheric oxygen, and others remain unfilled. In both cases, the reaction increases. The filled vacancies (with oxygen atoms) will add additional oxygen sites so that H₂S will collide with more oxygen atoms and react as in Eq. (1). The remaining unfilled vacancies with Al dangling bonds trap H₂S molecules, making an increase in the reaction rate that finally increases the sensor response. All these reactions are governed by the rise in diffusion that depends itself (diffusion) on temperature. The steepness of the decrease in H₂S concentration (k_s) increases as the doping percentage increases. This is the reverse behavior of (T_0), which is the temperature at which the density of H₂S reaches half of its original density due to autoignition. Finally, the parameter (C) that correlates the resistance with the reaction rate increases as the doping percentage rises due to imperfections in the ZnO lattice caused by doping. The last reaction does not include autoignition parameters because the O_2 gas does not have autoignition temperature, and the percentage of O_2 in the air is nearly constant.

Conclusions

Theoretical simulation of gas sensors rarely deals with calculating response or recovery reaction kinetics of gas sensing. The present model uses transition state, including its DFT tool, to calculate reaction rate, response, response time, and recovery time. The results as a function of temperature are in good agreement with the experiment. The present model describes the sensing mechanism as interplay between the reaction of the detected gas (H₂S) with the sensitive material (pure or Al-doped ZnO) or the reaction of the oxygen-deficient detection material with O_2 in air. As the temperature approaches the autoignition temperature, the detected gas prefers the reaction with O_2 in the air before reaching the sensitive material. The maximum response value is at a temperature just below the autoignition temperature. The temperature dependence of the reaction of H₂S is more robust as the Al doping increases to reach the optimum doping percentage at 4 %.

The temperature dependence of the reaction of H_2S with O_2 in the air becomes more robust as the optimum doping percentage at 4 % Al is reached. This indicates that Al doping increases H_2S reaction with the sensitive material and also increases the reaction of H_2S with O_2 in the air due to lattice distortion.

Author Information*

_____

*The authors' names are presented in the following order: First Name, Middle Name and Last Name

Mudar Ahmed Abdulsattar — Chief Scientific Researcher, Head of Solid-State Department, Ministry of Science and Technology, Rusafa Street, 52, 10045, Baghdad, Iraq, e-mail: mudarahmed3@yahoo.com; https://orcid.org/0000-0001-8234-6686

Sawsan Mudar Almaroof — Senior Engineer, Information Technology Department, Engineering Construction Office, Ministry of Construction, Housing, Municipalities and Public Works, Baghdad Governorate, 10011, Baghdad, Iraq; e-mail: sawsanalmaroof@outlook.com

Author Contributions

The manuscript was written through contributions of all authors. All authors have given approval to the final version of the manuscript. CRediT: **Mudar Ahmed Abdulsattar** — supervision, data curation, methodology, review & editing, **Sawsan Mudar Almaroof —** investigation, formal analysis, writing-original draft.

Conflicts of Interest

The authors declare no conflict of interest.

References

1   Noman, M.T., Amor, N., & Petru, M. (2022). Synthesis and Applications of ZnO Nanostructures (ZONSs): A Review. *Critical Reviews in Solid State and Materials Sciences*, *47*, 99–141. https://doi.org/10.1080/10408436.2021.1886041.

2   Vanga, S.R., & Sarada, V. (2022). Improving sensitivity of ZnO nanorods for the application of gas sensors at low temperatures: a review. *Proceedings — 2nd International Conference on Next Generation Intelligent Systems*, ICNGIS 2022. https://doi.org/10.1109/ICNGIS54955.2022.10079894.

3   Zhang, L., Kang, Y., Tang, Y., & Yu, F. (2024). UV-Activated ZnO–NiO Heterojunction Sensor for Ethanol Gas Detection at Low Working Temperature. *Materials Science in Semiconductor Processing*, *169*. https://doi.org/10.1016/j.mssp.2023.107925.

4   Abdelkarem, K., Saad, R., El Sayed, A.M., Fathy, M.I., Shaban, M., & Hamdy, H. (2023). Design of High-Sensitivity La-Doped ZnO Sensors for CO_2 Gas Detection at Room Temperature. *Scientific Reports*, *13*. https://doi.org/10.1038/s41598-023-45196-y.

5   Feng, Z., Wang, H., Zhang, Y., Han, D., Cheng, Y., Jian, A., & Sang, S. (2023). ZnO/GaN n-n Heterojunction Porous Nanosheets for Ppb-Level NO_2 Gas Sensors. *Sensors and Actuators B: Chemical*, *396*. https://doi.org/10.1016/j.snb.2023.134629.

6   Kolhe, P.S., Shinde, A.B., Kulkarni, S.G., Maiti, N., Koinkar, P.M., & Sonawane, K.M. (2018). Gas Sensing Performance of Al Doped ZnO Thin Film for H_2S Detection. *Journal of Alloys and Compounds*, *748*, 6–11. https://doi.org/10.1016/j.jallcom.2018.03.123.

7   Kumar, S., Lawaniya, S.D., Agarwal, S., Yu, Y.-T., Nelamarri, S.R., Kumar, M., Mishra, Y.K., & Awasthi, K. (2023). Optimization of Pt Nanoparticles Loading in ZnO for Highly Selective and Stable Hydrogen Gas Sensor at Reduced Working Temperature. *Sensors and Actuators B: Chemical*, *375*. https://doi.org/10.1016/j.snb.2022.132943.

8   Xuan, J., Wang, L., Zou, Y., Li, Y., Zhang, H., Lu, Q., Sun, M., Yin, G., & Zhou, A. (2022). Room-Temperature Gas Sensor Based on in Situ Grown, Etched and W-Doped ZnO Nanotubes Functionalized with Pt Nanoparticles for the Detection of Low-Concentration H2S. *Journal of Alloys and Compounds*, *922*. https://doi.org/10.1016/j.jallcom.2022.166158.

9   Abdulsattar, M.A. (2020). Transition State Theory Application to H_2 Gas Sensitivity of Pristine and Pd Doped SnO_2 Clusters. *Karbala International Journal of Modern Science*, 6, 13. https://doi.org/10.33640/2405-609X.1615.

10 Abdulsattar, M.A. (2023). The Reaction of Pristine and Rh-Doped SnO_2 Clusters with Acetone: Application of Evans–Polanyi Principle to Transition State Theory. *Journal of Molecular Modeling*, *29*. https://doi.org/10.1007/s00894-023-05710-5.

11 Abdulsattar, M.A. (2023). $Ga_xIn_{2-x}XO_3$ Surface Pyramids Interaction with Formaldehyde: Thermodynamic and Sensing Analysis. *Karbala International Journal of Modern Science*, *9*, 8. https://doi.org/10.33640/2405-609X.3324.

12 Abdulsattar, M.A. (2015). Capped ZnO (3, 0) Nanotubes as Building Blocks of Bare and H Passivated Wurtzite ZnO Nanocrystals. *Superlattices and Microstructures*, *85*, 813–819. https://doi.org/10.1016/j.spmi.2015.07.015.

13 Abdulsattar, M.A., Abduljalil, H.M., & Abed, H.H. (2022). Effect of Au Doping on ZnO Nanoparticles Sensitivity to Ethanol: A Thermodynamic and Density Functional Theory Study. *New Materials, Compounds and Applications*, *6*, 230–242.

14 Hasan, F.A., & Hussein, M.T. (2021). Study of Some Electronic and Spectroscopic Properties of ZnO Nanostructers by Density Functional Theory. *Materials Today*: *Proceedings*, 2638–2644. https://doi.org/10.1016/j.matpr.2020.12.593.

15 Mousavi, S.P., Nakhaei-Kohani, R., Atashrouz, S., Hadavimoghaddam, F., Abedi, A., Hemmati-Sarapardeh, A., & Mohaddespour, A. (2023). Modeling of H2S Solubility in Ionic Liquids: Comparison of White-Box Machine Learning, Deep Learning and Ensemble Learning Approaches. *Scientific Reports*, *13*. https://doi.org/10.1038/s41598-023-34193-w.

16 Kanth, S., Chikara, A.K., Choudhury, S., & Betty, C.A. (2023). Portable and Room Temperature Operating H2S Gas Detection and Alert System Using Nanocrystalline SnO_2 Thin Films. *IEEE Sensors Letters*, *7*. https://doi.org/10.1109/LSENS.2023.3267510.

17 Hydrogen Sulfide (2023). Wikipedia. https://en.wikipedia.org/wiki/Hydrogen_sulfide.

18 Li, L., & King, D.L. (2006). H2S Removal with ZnO during Fuel Processing for PEM Fuel Cell Applications. *Catalysis Today*, *116*, 537–541. https://doi.org/10.1016/j.cattod.2006.06.024.

19 Novochinskii, I.I., Song, C., Ma, X., Liu, X., Shore, L., Lampert, J., & Farrauto, R.J. (2004). Low-Temperature H2S Removal from Steam-Containing Gas Mixtures with ZnO for Fuel Cell Application. 1. ZnO Particles and Extrudates. *Energy and Fuels*, *18*, 576–583. https://doi.org/10.1021/ef030137l.

20 Yang, X.Y., Zhang, W.J., Yue, L.J., Xie, K.F., Jin, G.X., Fang, S.M., & Zhang, Y.H. (2023). Co Sites Induced Synergistic Effect in Hollow Co_3O_4/ZnO Nanocage for Enhanced H2S Sensing Performance. *Applied Surface Science*, *640*. https://doi.org/10.1016/j.apsusc.2023.158417.

21 To, D.T.H., Park, J.Y., Yang, B., Myung, N.V., & Choa, Y.H. (2023). Nanocrystalline ZnO Quantum Dot-Based Chemiresistive Gas Sensors: Improving Sensing Performance towards NO_2 and H2S by Optimizing Operating Temperature. *Sensors and Actuators Reports*, *6*. https://doi.org/10.1016/j.snr.2023.100166.

22 Li, X., Jia, F., Luo, N., Cai, H., Chen, J., Ren, W., Cheng, J., & Xu, J. (2024). Self-Assembly Tourmaline@$BiFeO_3$ Composites with Enhanced Polarization for Dual-Selective C_3H_6O and H2S Detection. *Sensors and Actuators B: Chemical*, *399*. https://doi.org/10.1016/j.snb.2023.134806.

23 Kumar, N., Jasani, J., Sonvane, Y., Korvink, J.G., Sharma, A., & Sharma, B. (2024) Unfolding the Hydrogen Gas Sensing Mechanism across 2D Pnictogen/Graphene Heterostructure Sensors. *Sensors and Actuators B: Chemical*, *399*. https://doi.org/10.1016/j.snb.2023.134807.

24 Frisch, M.J., Trucks, G.W., Schlegel, H.B., Scuseria, G.E., Robb, M.A., Cheeseman, J.R., Scalmani, G., Barone, V., Mennucci, B., Petersson, G.A., Nakatsuji, H., Caricato, M., Li, X., Hratchian, H.P., Izmaylov, A.F., Bloino, J., Zheng, G., Sonnenberg, J.L., Hada, M., Ehara, M., Toyota, K., Fukuda, R., Hasegawa, J., Ishida, M., Nakajima, T., Honda, Y., Kitao, O., Nakai, H., Vreven, T., Montgomery, J.A.J., Peralta, J.E., Ogliaro, F., Bearpark, M., Heyd, J.J., Brothers, E., Kudin, K.N., Staroverov, V.N., Kobayashi, R., Normand, J., Raghavachari, K., Rendell, A., Burant, J.C., Iyengar, S.S., Tomasi, J., Cossi, M., Rega, N., Millam, J.M., Klene, M., Knox, J.E., Cross, J.B., Bakken, V., Adamo, C., Jaramillo, J., Gomperts, R., Stratmann, R.E., Yazyev, O., Austin, A.J., Cammi, R., Pomelli, C., Ochterski, J.W., Martin, R.L., Morokuma, K., Zakrzewski, V.G., Voth, G.A., Salvador, P., Dannenberg, J.J., Dapprich, S., Daniels, A.D., Farkas, Ö., Foresman, J.B., Ortiz, J. V., Cioslowski, J., & Fox, D.J. (2013). Gaussian 09, Revision D.01. Gaussian, Inc., Wallingford CT.

25 Abdulsattar, M.A., Almaroof, H.M., & Almaroof, N.M. (2020). Transition State Theory Application to ZnO Nanocluster Sensitivity to H2 Gas. *Optik*, *219*. https://doi.org/10.1016/j.ijleo.2020.165278.

26 Abdulsattar, M.A., Jabbar, R.H., Abed, H.H., & Abduljalil, H.M. (2021). The Sensitivity of Pristine and Pt Doped ZnO Nanoclusters to NH3 Gas: A Transition State Theory Study. *Optik*, *242*. https://doi.org/10.1016/j.ijleo.2021.167158.

27 Abdulsattar, M.A. (2024). Effect of Acetylene Properties on Its Gas Sensing by NiO Doped ZnO Clusters: A Transition State Theory Model. *Eurasian Journal of Chemistry*, *29*, 35–43. https://doi.org/10.31489/2959-0663/4-24-8.

28 Abdulsattar, M.A., & Mahmood, T.H. (2023). Enhancement of SnO_2 Sensitivity to Acetone by Au Loading: An Application of Evans–Polanyi Principle in Gas Sensing. *Optik*, *275*, 170604. https://doi.org/10.1016/j.ijleo.2023.170604.

29 Hosseinpour, P. (2020). Effect of Gaussian Impurity Parameters on the Valence and Conduction Subbands and Thermodynamic Quantities in a Doped Quantum Wire. *Solid State Communications*, 322. https://doi.org/10.1016/j.ssc.2020.114061.

30 Misják, F., Nagy, K.H., Lobotka, P., & Radnóczi, G. (2014). Electron Scattering Mechanisms in Cu-Mn Films for Interconnect Applications. *Journal of Applied Physics*, *116*. https://doi.org/10.1063/1.4893718.